minerals

MDPI

Review

Amp-TB2 Protocol and Its Application to Amphiboles from Recent, Historical and Pre-Historical Eruptions of the Bezymianny Volcano, Kamchatka

Filippo Ridolfi [1,*], Renat R. Almeev [1], Alexey Yu Ozerov [2] and Francois Holtz [1]

[1] Institut für Mineralogie, Faculty of Natural Sciences, Leibniz University Hannover, Callinstrasse 3, 30167 Hannover, Germany; r.almeev@mineralogie.uni-hannover.de (R.R.A.); f.holtz@mineralogie.uni-hannover.de (F.H.)
[2] Institute of Volcanology and Seismology, Piip Boulevard 9, Petropavlovsk-Kamchatsky 683006, Russia; ozerov@kscnet.ru
* Correspondence: f.ridolfi@mineralogie.uni-hannover.de

Abstract: This article reports a protocol on the application of Amp-TB2 (single-amphibole thermobarometry) based on detailed electron-microprobe analyses performed on homogeneous natural standards and synthetic glasses, and amphibole crystals (mostly phenocrysts) of volcanic products erupted by the Bezymianny volcano during its activity through time. The application of this protocol is facilitated by a new version of the model (Amp-TB2.1.xlsx) including an equation to identify heterogeneous domains (disequilibrium; not suitable for thermobarometric constraints) and homogenous (equilibrium) zones within amphibole crystals, which can be used to quantify the physicochemical parameters (i.e., pressure, P; temperature, T; volatile content in the melt, H_2O_{melt}; oxygen fugacity, fO_2) of "steady-state" magmatic crystallization. Application examples of the protocol, showing detailed core–rim microprobe data and physicochemical parameter variations in representative amphibole phenocrysts of the Bezymianny are also reported. The depth (and P) estimated by Amp-TB2.1 for this volcano are compared to seismic tomography results. Amp-TB2.1 results mainly show (1) that the Bezymianny is characterized by a very dynamic feeding system where the magma is stored at shallow crustal levels before recent activity periods characterized by climatic events and (2) that the pre-eruptive depth of magma storage generally increases with the age of the investigated products.

Keywords: amphibole; homogeneous domains; thermobarometry; equilibrium crystallization; volcanoes; magma chamber; magma-feeding system; seismic tomography

Citation: Ridolfi, F.; Almeev, R.R.; Ozerov, A.Y.; Holtz, F. Amp-TB2 Protocol and Its Application to Amphiboles from Recent, Historical and Pre-Historical Eruptions of the Bezymianny Volcano, Kamchatka. *Minerals* **2023**, *13*, 1394. https://doi.org/10.3390/min13111394

Academic Editor: Federica Zaccarini

Received: 28 September 2023
Revised: 19 October 2023
Accepted: 28 October 2023
Published: 30 October 2023

1. Introduction

Amp-TB2 is a single-phase thermobarometric model for estimating the physicochemical crystallization conditions of Ca- and Mg-rich amphiboles (Amp) in calc-alkaline and alkaline igneous rocks across a wide P–T range (up to 2200 MPa and 1130 °C) and with relatively low uncertainties (P ± 12%, T ± 22 °C, logfO_2 ± 0.3, H_2O_{melt} ± 14%; [1]). It provides warnings whenever the input composition is incorrect or diverges from that of the calibration data and includes diagrams for an easy graphical representation of the results.

This model is the last of a series of thermobarometric applications where Ridolfi and co-authors progressively increased the accuracy and extended the validity of their thermobarometric formulations through the selection of consistent and "high-quality" experimental data and tested the capability of the Amp to recover the physicochemical conditions of "steady-state" (equilibrium) magmatic crystallization [2–7]. A "steady-state" condition of magma crystallization is meant as a nearly stable magmatic environment where changes in intrinsic parameters, melt and mineral compositions fall within the analytical and thermobarometric uncertainties. The main aim of Ridolfi and co-authors was to retrieve barometric equations capable of defining crustal-level magma chambers of active

and quiescent volcanoes, and to test their validity by comparing the estimated depths (and P) of magma reservoirs with those of complementary and independent methods, such as seismicity and seismic tomography, e.g., [8–11].

Ridolfi et al., in 2008 [2], proposed the first single-Amp barometric and fO_2 equations valid for intermediate–basic calc-alkanline magmas. These equations allowed them to define the conditions and depth amplitude (from ca. 7 to 11 km) of the andesite magma chamber of the El Reventador volcano, that started a new eruptive cycle in 3 November 2002 after 26 years of quiescence, by the intrusion of a basic magma at the base of the chamber (as inferred by a 4.1 magnitude volcano–tectonic earthquake with a hypocenter depth of ~11 km on 6 October 2002; [2,3]).

Ridolfi et al., in 2010 [3], reported an overview of the crystallization of amphiboles in calc-alkaline magmas and new single-Amp thermobarometric equations, including some testing with independent but complementary methodologies, such as pre-eruptive seismicity (volcano–tectonic earthquake locations and frequency), seismic tomography, Fe–Ti oxides, amphibole–plagioclase, plagioclase–liquid equilibria thermobarometry and melt inclusion studies.

In 2012, Ridolfi and Renzulli [4] tested previous Amp thermobarometers using "high-quality" experimental results (in which compositional data are provided with relatively low uncertainties and are consistent with the natural ones) obtained from calc-alkaline and alkaline starting materials, and extended the validity of Amp thermobarometry to alkaline magmas and P–T conditions up to 1130 °C and 2.2 GPa.

Other validations on the capability of Amp thermobarometry to recover the pressure (P) and depth of shallow magma chambers underneath active volcanoes are reported by independent researchers, e.g., [12–19]. In addition, Ridolfi et al. [7] published a mass-based method to obtain the formula parameters of Na, Na-Ca, Ca and oxo amphiboles from electron-microprobe (EPMA) analyses with a precision two to four times that of classic Amp formula calculation approaches. The authors also attached a user-friendly spreadsheet (AMFORM.xlsx) reporting warnings for bad analyses and large deviations from the ideal total element oxide and correct stoichiometry.

Some suggestions to avoid the incorrect application of Amp thermobarometry, and thus avoiding unreliable results, are reported in [5,6]. In particular, these authors stated that intra-crystalline compositional and textural variations can be used to identify chemically homogeneous amphibole domains, indicative of "steady-state"magmatic crystallization, and to distinguish them from heterogeneous zones resulting from disequilibrium crystallization or from element diffusion at the crystal–melt interface sub-volcanic processes, e.g., magma mixing, ascent and convection. However, the threshold between homogeneous and heterogeneous domains in amphiboles measured by electron-probe microanalysis (EPMA) and the extent to which Amp thermobarometry can be safely applied have not been fully defined. In addition, "apparent" heterogeneities in replicate measurements of originally homogeneous amphiboles can be the result of uncertain analytical data (bad or loss of focusing during serial analyses, contamination from an adjacent phase, small inclusions that cannot be easily identified, etc.).

In this work, we define a threshold between homogeneous and heterogeneous compositions, and propose a protocol for the application of Amp-TB2 based on EPMA data of amphiboles from the recent, historical and pre-historical erupted products of the Bezymianny volcano (Kamchatka), e.g., [20–25]. We show that the application of this protocol can lead to great details on the magma-storage locations and processes, and their variations through time, underneath active volcanoes.

2. Homogeneous vs. Heterogeneous Domains

2.1. Threshold between Heterogeneous and Homogeneous Compositions as Measured by EPMA

In order to find a criterion to exclude problematic analyses of amphiboles and establish a threshold between homogeneous and heterogeneous compositional domains, we have performed multiple EPMA measurements (from 10 to 30 analyses along profiles or at differ-

ent spots) using a set of mineral and glass standards (Smithsonian Institution) and synthetic glasses with different compositions (which so far are considered to be homogeneous, i.e., shows intra-crystal chemical variations within the uncertainty of EPMA measurements; e.g., [26]), and calculated the average amount of element oxides (in wt%), the relative standard deviation (σ, in wt%) and its percentage value (σ% = σ wt% × 100/element oxide wt%; Figure 1a). Independent of the measured element oxide (i.e., SiO_2, TiO_2, Al_2O_3, Cr_2O_3, FeO_{tot}, MnO, MgO, CaO, Na_2O and K_2O), their averaged amount and EPMA setting (e.g., choice of analyzer crystals, current intensity and beam size), we found that the σ% values decrease with the concentration of the measured element oxide (wt%), as follows:

$$\sigma\% = 5.7628 \times \text{element oxide wt\%}^{-0.661} \ (R^2 = 0.8038) \quad (1)$$

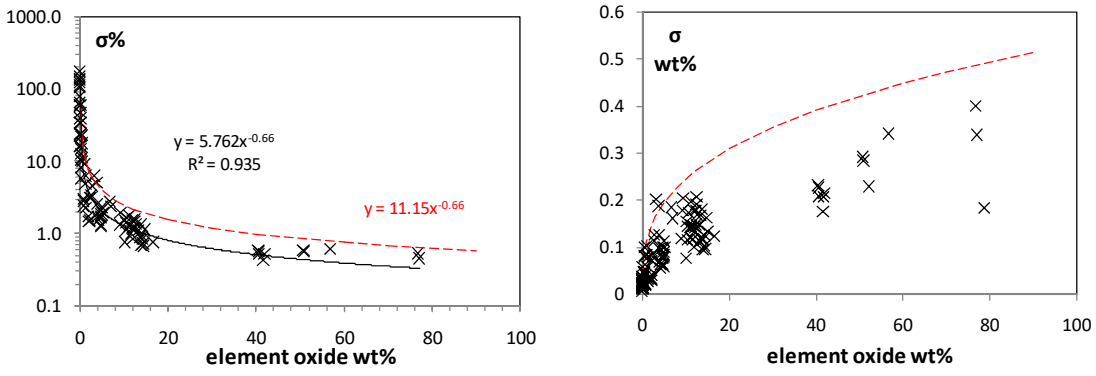

(**a**) (**b**)

Figure 1. (**a**) Correlation between the standard deviation percentage of different element oxides (σ% = σ wt% × 100/measured element oxide wt%) and the element oxide wt% of multiple EPMA measures (10–30 spot EMP analyses for each standard) on "homogeneous" Smithsonian microbeam standards (minerals and glasses: Kakanui hornblende 143,965, Arenal hornblende NMNH 111,356, Diopside NMNH 117,733, Kakanui Augite NMNH 122,142,VG-568 rhyolite NMNH 72,854, VG-A99 basalt NMNH 113, 498-1; e.g., [26]) and glasses synthesized at 1600 °C and air conditions (i.e., high-K rhyolite, basaltic andesite and basalt) using the Cameca SX 100 of the University of Hannover with different EPMA settings (black curve). The red-dashed curve reports this power relationship multiplied by a factor of 2. Related equations are reported with the same color; (1) and (2) in the text. The relationship described by Equation (2) is also reported in (**b**), showing the standard deviation values (σ in wt%) of different element oxides vs. the element oxide wt% of the phases reported above. The diagrams show that homogeneous mineral and glass samples, containing major oxides in a wide concentration range, are mostly characterized by lower σ% and σ values than those of Equation (2) (red-dashed curve).

This relationship basically represents the averaged precision based on 10 measured oxides characterizing the quality of the EPMA and the degree of homogeneity of the used samples.

Figure 1a also shows the pattern of a curve equal to (1) multiplied by a factor of two (red-dashed curve), i.e.,:

$$\sigma\% = 11.153 \times \text{element oxide wt\%}^{-0.661} \quad (2)$$

It is worth noting that all measured homogeneous standards and glasses show the σ% values ≤ to those calculated by Equation (2) for most of the measured element oxides. This relationship can then be used to distinguish homogeneous phases or intra-crystal domains from heterogeneous ones (see below).

In other words, homogeneous compositions should show the σ% of all their element oxides lower than or equal to a threshold calculated by Equation (2), whereas heterogeneous compositions are invariably characterized by higher uncertainties. It is worth noting that

"homogeneity" is a scale-dependent concept depending on the length scale of the analytical method and the sample/s used to test it. In the case reported in this work, homogeneity is defined by the interaction of an EPMA (i.e., Cameca SX100, operating in profile analysis) with minerals and glasses assumed to have intra-crystal compositional consistency of their major elements (Figure 1). In addition, this condition is also respected by the JEOL JXA-iHP 200F EPMA (recently installed at Leibniz University Hannover), as all mineral and glass standards measured so far show σ% values ≤ to those estimated by Equation (2).

The σ values calculated with (2) are 0.47 wt% at a level of the measured element oxide of 70 wt%, 0.42 at 50 wt%, 0.39 at 40 wt%, %, 0.31 wt% at 20 wt%, 0.24 wt% at 10 wt%, 0.19 wt% at 5 wt%, 0.14 wt% at 2 wt%, 0.11 wt% at 1 wt% and 0.05 wt% at 0.1 wt% levels. This pattern is also reported in Figure 1b, showing that most of the measured element oxides have σ values lower than those predicted by Equation (2) (red-dashed curve).

It is worth noting that Equation (2) was recently used by Ridolfi [1] to select the "high-quality" dataset of experimental amphiboles for refining his Amp-TB2 model.

2.2. Intra-Crystal Analysis of Amp Composition and Related Physicochemical Parameters

Figures 2–5 show the back-scattered electron (BSE) images and core–rim intra-crystal EPMA profiles of representative amphibole phenocrysts from different eruptive products of the Bezymianny volcano (see Section 4 and Supplementary Materials Table S1 for additional information). Core–rim variations of physicochemical parameters (i.e., pressure, P; temperature, T; oxygen fugacity expressed as difference from the Ni-NiO buffer, ΔNNO; volatile content in the melt, H_2O_{melt}) are also shown in all figures. These conditions were calculated with Amp-TB2 that is attached to this work in a modified version, including Equation (2) and intra-crystal compositional analyses of the Bezymianny Amp phenocrysts in Figures 2–5. (i.e., Amp-TB2.1.xlsx; Supplementary Materials). Overall, the representative zoned phenocrysts show large compositional variations that are well above the homogeneity threshold provided by Equation (2). Nevertheless, in the core, mantle and rim zones of all phenocrysts, homogeneous intra-crystal domains (with σ%~≤ (2) for all measured element oxides) are found alternating with heterogeneous ones (with σ% > (2) for the main element oxides), indicating that the Amp underwent stages of equilibrium ("steady-state") crystallization alternating with disequilibrium (kinetic) modifications (Supplementary Materials).

Figure 2 reports the intra-crystal analysis of a phenocryst in the Amp-bearing andesite sample from the Novy lava dome in the central crater of the Bezymianny volcano (extruded in 1990). The phenocryst appears to be apparently homogeneous in the BSE imaging. However, the EPMA indicates three homogeneous domains (core, mantle and rim) describing normal zoning, i.e., where the amount of Al_2O_3 (that is reversely correlated to SiO_2) and Na_2O decreases from core to rim, along with P (487 ± 23, 374 ± 13, 230 ± 16 MPa), T (937 ± 10, 910 ± 8, 852 ± 0.3 °C) and H_2O_{melt} (7.2 ± 0.3, 6.6 ± 0.1, 6.3 ± 0.3 wt%), indicative of periods of magma stagnation ("steady-state" equilibrium crystallization) at three different crustal levels. MgO and FeO_{tot} variations go along with the relative oxygen fugacity (ΔNNO, e.g., [2,27]) that is higher at the core (0.8 ± 0.2 log units), and do not vary from mantle to rim (0.3 ± 0.2 and 0.4 ± 0.3 log units, respectively). In the heterogeneous zones, P, T and fO_2 roughly follow the pattern shown by the normal domains, suggesting magma ascent. Nevertheless, the values of σ for Al_2O_3 and FeO_{tot} are much higher than those calculated with (2), and thus the physicochemical parameters cannot be quantitatively constrained (Supplementary Materials). The breakdown corona indicates that the phenocryst was brought at conditions outside the Amp stability field during its ascent to the surface.

Figure 3 shows the intra-crystal analysis of a twin phenocryst coming from another sample of the same lava dome extrusion. The BSE image shows evident zoning for the left side of the crystal, with brightness progressively increasing towards the rim. Two homogeneous domains (core and rim) are easily distinguishable, indicating different conditions (706 ± 60 MPa, 971 ± 13 °C, ΔNNO + 2.2 ± 0.4, 8.0 ± 0.3 wt% H_2O_{melt} vs. 246 ± 16 MPa,

874 ± 7 °C, ΔNNO + 0.8 ± 0.2 log units, 5.8 ± 0.2 wt% H_2O_{melt}) and suggesting the ascent of the magma through the crust. Magma ascent is also suggested by the heterogeneous domain, where the composition and physicochemical parameters gradually vary from core to rim. However, the σ% values calculated for this zone are much higher than (2) for Al_2O_3, FeO_{tot} and MgO, and the P and logfO_2 standard deviations (20% and 0.9 log units) are well above those predicted by Amp-TB2 (12% and 0.3 log units, respectively; Supplementary Materials). The gradual–diffusive compositional variation from core to rim could be due to a re-equilibration process in the crust by the contact with a more silicic melt, e.g., [28–31], or a constant-speed magma ascent, where the Amp grew in contact with a melt, gradually cooling down and evolving to silicic compositions.

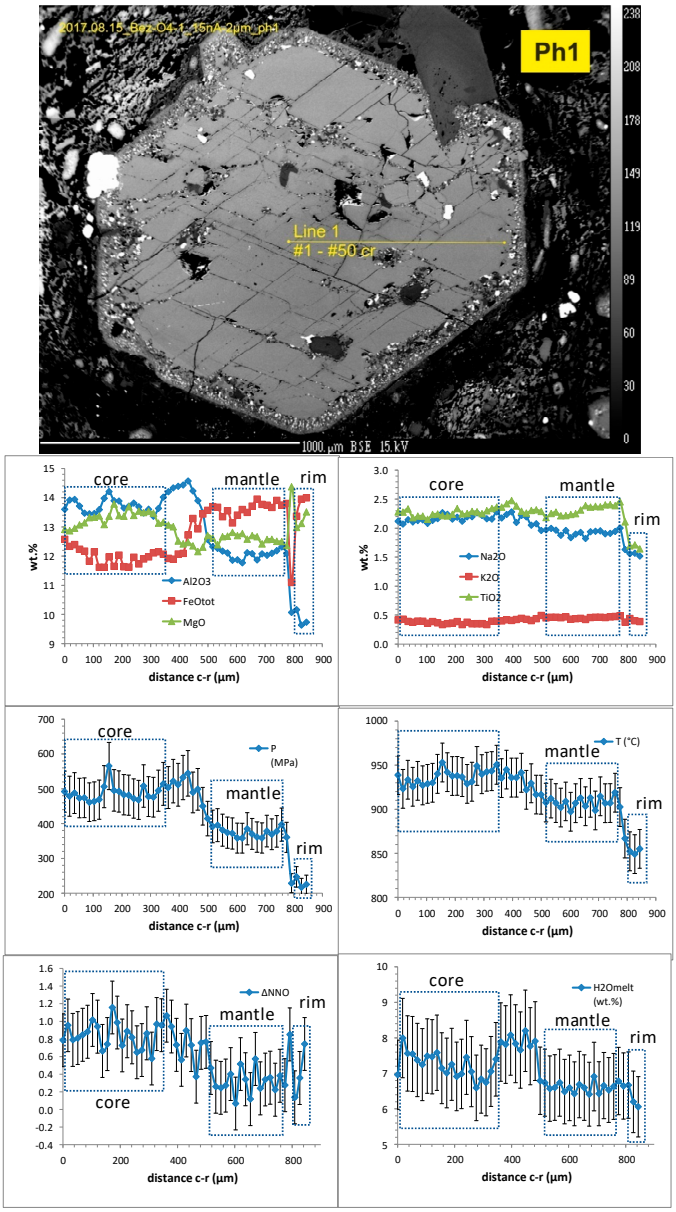

Figure 2. BSE image and core–rim quantitative EPMA profiles of an amphibole phenocryst from a Novydome 1990 extrusion (sample Bez O4-1). The phenocryst is characterized by a thin breakdown rim. The dotted boxes indicate compositionally homogeneous domains (i.e., σ% ~≤ 11.153 x element oxide wt%$^{-0.661}$; i.e., Equation (2)) and reliable Amp-TB2 physicochemical conditions (i.e., T σ ≤ 23 °C, P σ% ≤ 12%, ΔNNO σ ≤ 0.3, H_2O_{melt} σ% ≤ 14%). The bar errors in the T, P, ΔNNO and H_2O_{melt} vs. core–rim distance diagrams indicate these Amp-TB2 statistics uncertainties.

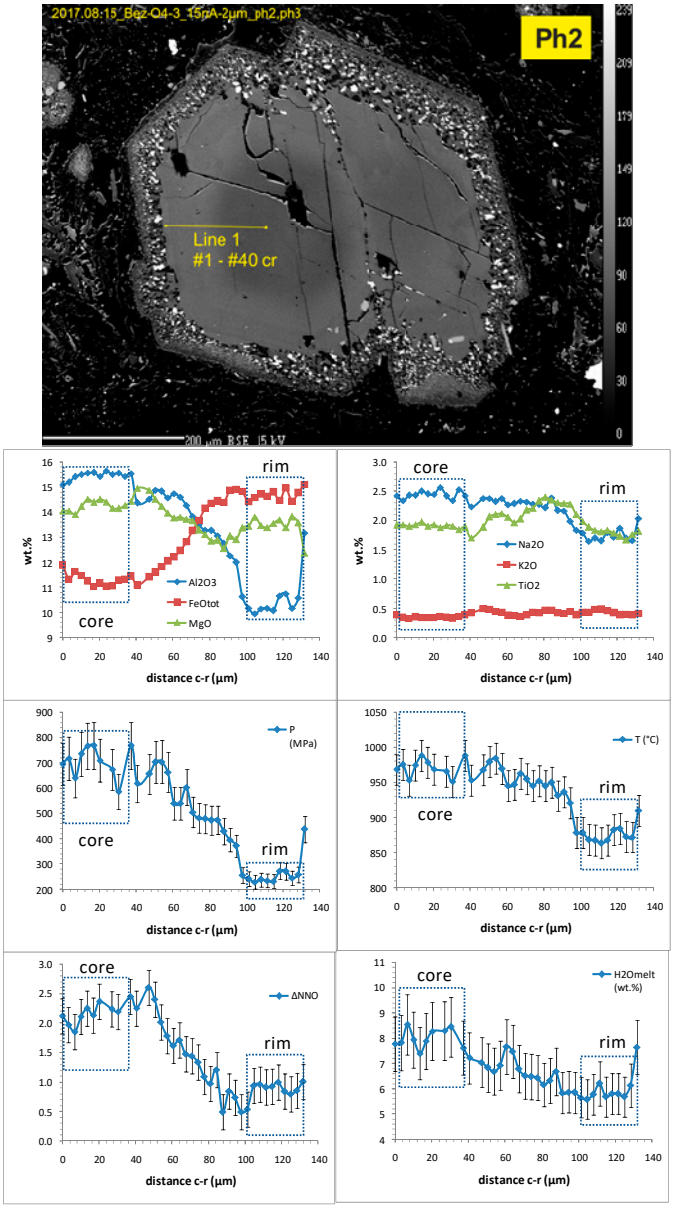

Figure 3. BSE image and core–rim quantitative EPMA profiles of an amphibole phenocryst from a Novy dome 1990 extrusion (sample Bez O4-3). The phenocryst is characterized by a thin breakdown rim. See Figure 2 for additional explanations.

Figure 4 shows an Amp phenocryst from the historical products of the Bezymianny (1–1.35 kys BP, Lochmaty lava dome) with a very complex zoning. However, four homogeneous domains can be identified with the application of Equation (2) (core, mantle 1, mantle 2 and rim). Despite its complexity, Al_2O_3, TiO_2 and Na_2O do not show large variations from core to mantle 2, with the calculated P–T–H_2O_{melt} conditions (543–603 MPa, 950–970 °C, 7.2–7.3 wt%) varying well within the uncertainties of Amp-TB2. At the homogeneous rim zone, slight decreases of P (498 ± 26 MPa) and T (925 ± 9 °C) come along with an increase of H_2O_{melt} (8.1 ± 0.5 wt%). The main compositional variations are due to MgO and FeO_{tot} correlated with large fO_2 variations (core = −9.4 ± 0.3, mantle 1 = −8.7 ± 0.2, mantle 2= –9.3 ± 0.3, rim = –10.1 ± 0.2 log units) (Supplementary Materials). It is worth noting that the phenocryst does not show any breakdown rim, and the calculated P goes down to 380 MPa at its rim (Figure 4). All of this suggests that the phenocryst grew in a magma zone at 400–600 MPa, where its process of crystallization was affected by hot fluids/melts coming from deeper zones, and was finally rapidly ejected to the surface.

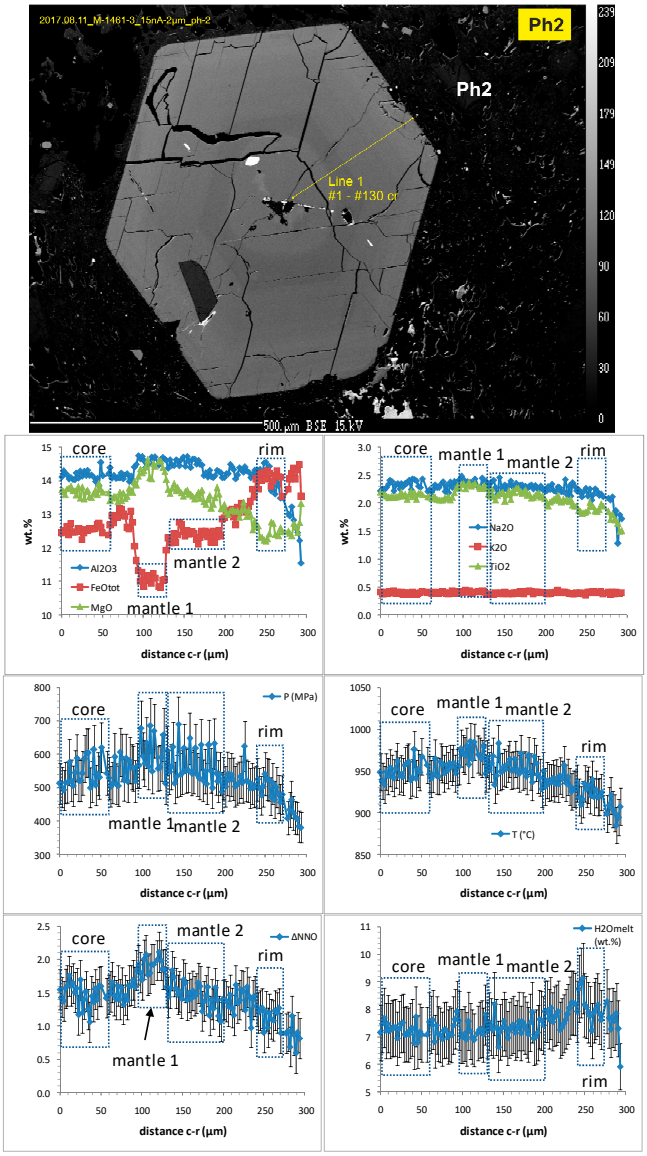

Figure 4. BSE image and core–rim quantitative EPMA profiles of an amphibole phenocryst from the lava dome Lokhmaty (sample M1461/3) extruded by the Bezymianny volcano at 1–1.35 kys BP. It is worth noting that the phenocrysts do not show any sign of breakdown at its rim. See Figure 2 for additional explanations.

Figure 5 shows another Amp phenocryst characterized by complex zoning and no breakdown corona from the old historical products of the Bezymianny (3.3–5.5 kys BP, lava dome Expeditsii). It is characterized by three homogeneous domains, where Al_2O_3 increases reversely from core to rim 1 and decreases (normal zoning) from rim 1 to 2. This variation is accompanied by an increase of equilibrium P from 307 ± 9 MPa (core) to 459 ± 22 MPa (rim 1), followed by a decrease of ~100 MPa (rim 2, P = 379 ± 13 MPa). Gorini et al. [6] cautiously suggested avoiding the application of Amp thermobarometry to reverse zonings. However, this suggestion was due to the lack in their database of enough detailed core–rim EPMA profiles. Reverse zonings are common in the recent and old products of the Bezymianny, and consistent with depth and size of the magma chambers obtained by seismic tomography (see [23] and Section 4). A similar pattern is observed for H_2O_{melt} (core = 5.5, rim 1 = 7.2, rim 2 = 5.5 ± 0.3 wt%). From core to rim 1, T follows the same pattern of P (894 ± 7 and 936 ± 9 °C, respectively), but does not show substantial variations at rim 2 (943 ± 8 °C). ΔNNO shows a reverse relationship with P (core = 1.6 ± 0.4,

rim 1 = 1.2 ± 0.2, rim 2 = 1.6 ± 0.2 log units) (Supplementary Materials; Figure 5). Al_2O_3 decreases at the heterogeneous domain to increase again towards rim 1. This pattern suggests a process of inter-diffusion of aluminum and should be not considered for thermobarometric quantification. All of this calls for a period of convective cycling of the magma within a crust chamber in between 460 and 310 MPa, followed by a rapid ejection to the surface of the magma (as inferred by the absence of breakdown corona at the Amp phenocryst rim).

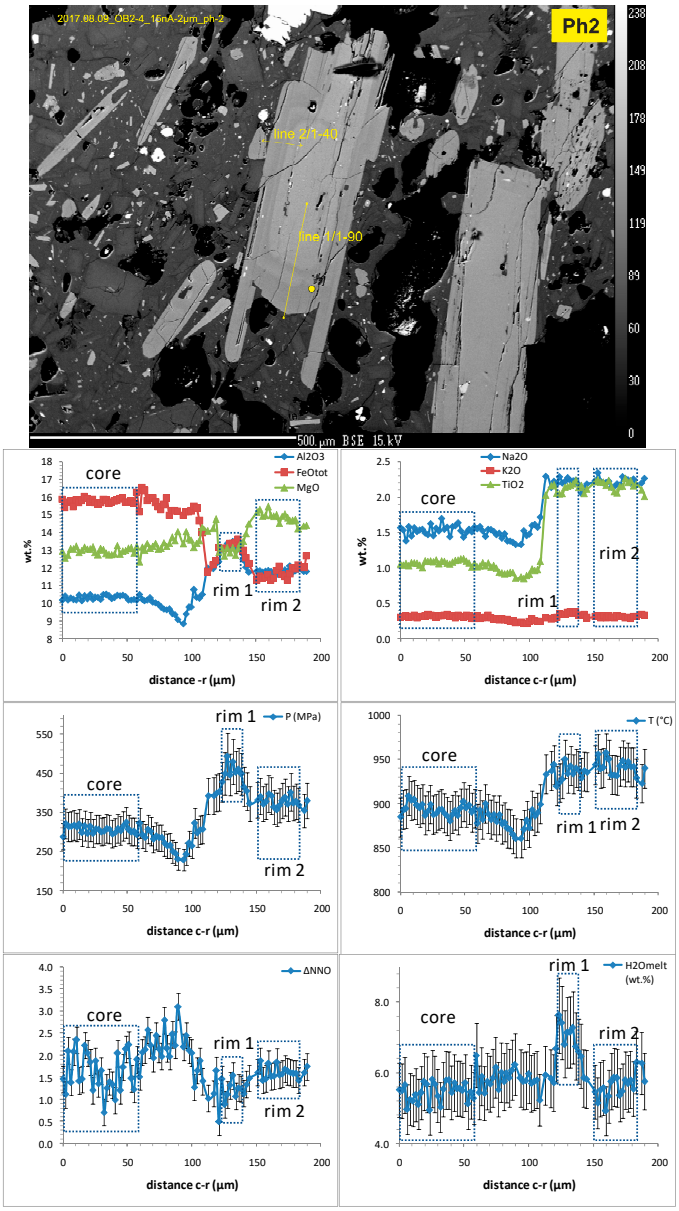

Figure 5. BSE image and core–rim quantitative EPMA profiles (line 1) of an amphibole phenocryst from the lava dome Expeditsii (Amp-bearing andesite, sample OB2/4) extruded by the Bezymianny volcano at 3.3–5.5 kys BP. It is worth noting that the phenocrysts do not show any sign of breakdown at its rim. See Figure 2 for additional explanations.

3. Protocol on the Application of Amp-TB2

This protocol is divided in three major steps, which should be followed consecutively in order to fully exploit the capability of Amp to recover the magmatic processes and related physicochemical variations, and to avoid misleading results.

3.1. Perform Detailed EPMA Profile

Independent of its igneous origin (plutonic vs. volcanic), detailed core–rim or rim–rim profile analyses through EPMA are highly recommended (e.g., Figures 2–5). Beam size and steps between the spot analyses should be as small as possible (typically 1 and 2 μm, respectively). Larger sizes should be chosen as a compromise between the size and homogeneity of the crystals, previously characterized by high-quality BSE imaging (e.g., Figures 2–5). EPMA quantitative measurements must include Si, Ti, Al, Cr, Fe, Mn, Mg, Ca, Na and K. Particular EPMA settings are not required, although a full characterization of Amp (including F and Cl) can be obtained following the procedure described in [26,32] (see Section 4 for the setting used in this work).

3.2. Check the Quality of the Amp Composition

Before applying Amp-TB2.1, it is highly recommended to check the quality of the Amp compositions using AMFORM.xlsx [7]. This is mostly done to prevent using low-quality data in the following steps, and to avoid inaccuracies. Compositions showing incorrect initial and final TEOs (total element oxides) and unbalanced stoichiometry should be discarded.

At this stage, it is convenient to input the compositional profiles into Amp-TB2.1 and perform a qualitative intra-crystal analysis by compositional, P, T, ΔNNO, H_2O_{melt} vs. profile-distance diagrams (Figures 2–5). In addition, we also recommend performing a final quality check. Indeed, although AMFORM.xlsx is a useful tool to avoid low-quality data, it is worth noting that its calibration also includes Na-Ca, Na and oxo amphiboles, and can fail to distinguish small compositional variations due to the contamination of the EPMA measure by small inclusions of other phases (glass, fluids or other minerals), or by the occurrence of unpredictable current jumps at the analyzer crystals. For this reason, it is recommended to carefully check on the textural/compositional relationship within the Amp crystals and discard data randomly diverging from the common compositional variations in the Amp (e.g., Figures 2–5).

3.3. Identify and Quantify Homgeneous Domains with Amp-TB2.1

Homogeneous and heterogeneous domains can be identified graphically and using Equation (2) that is included in the new version of the model (Amp-TB2.1.xlsx; Supplementary Materials). Other relevant changes in the new version concern the last step of the P calculation (i.e., xi; [1]), where P is determined by averaging Pb, Pc and Pd instead of P1a. This is to minimize the high uncertainties of P1a (20%), which is highly sensitive to sodium and can result in unrealistically high P values when the quality of the Na_2O analysis is low and/or when occasional current jumps occur at the related EPMA analyzer crystal (typically TAP, e.g., [26]). Uncertainties of Amp-TB2.1, as calculated on the experimental amphibole database (P ± 12%, T ± 23 °C, ΔNNO ± 0.3, H_2O_{melt} ± 14%), are nearly identical to those of the older version [1]. Finally, average and standard deviation values must be calculated also for the physicochemical parameter values given by the model in the zones constrained with Equation (2). The related σ and σ% values for the heterogeneous zones are generally higher than the uncertainties predicted by Amp-TB2.1. The physicochemical parameters of these heterogeneous domains cannot be quantitatively constrained. If an amphibole did not grow at "steady-state" (equilibrium) magmatic conditions, or underwent high degrees of post-magmatic alteration, it may not show any homogeneous domains. In this case, the calculated parameters do not have any qualitative and quantitative meaning. For homogeneous domains and unzoned amphiboles, σ and σ% must be ≤ to the uncertainties of the model. If these conditions are not verified, P1a should be manually inputted into the P cell for all the analyzed spots of the considered domain, allowing Amp-TB2.1.xlsx to adjust the other physicochemical parameters to the new input P. In this case, P σ% should be ≤ 20%.

Finally, the average and σ values obtained for each homogeneous domain can be plotted in the P–T, T–H_2O_{melt} and logfO_2–T diagrams in Amp-TB2 for a graphical representation and easy interpretation of the results (Figures 6 and 7; e.g., [5]).

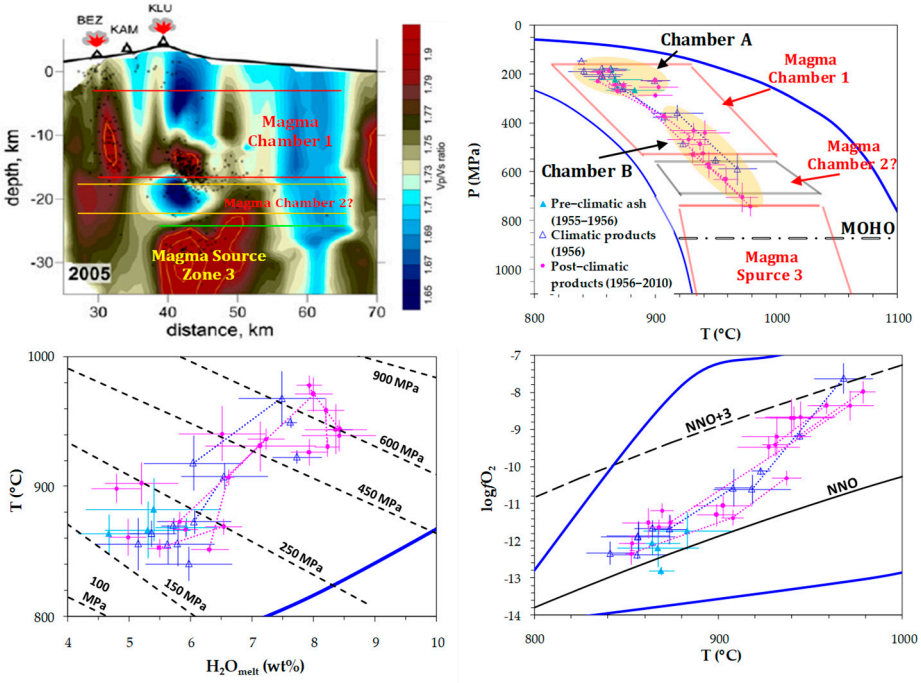

Figure 6. Comparison of tomography seismic imaging for an active period of the Bezymianny volcano (2005; image modified after [23]) with Amp-TB2.1 results for the recent products (1955–2010). The depth–distance diagram (tomography image) shows a shallow-crust magma chamber (1) underneath the Bezymianny and a magma source (3) below the Klyuchevskoy volcano, characterized by high Vp/Vs values. Underneath the Bezymianny, another zone with relatively high Vp/Vs ratios suggests the occurrence of a second magma chamber in the crust (Magma Chamber 2?), which can be arguably interpreted as an extension of Magma Chamber 1. The top of the Magma Chamber 1 is at 6 km, also postulated by [33] on the analysis of historical seismicity. These magma chambers are reported in the P–T diagram together with the MOHO (e.g., [34], also reporting two main storage regions), where the Amp crystallized at equilibrium conditions, i.e., Magma Chamber A and B (shaded-yellow fields). Depth–P conversion is calculated using a crust density of 2700 kg/m^3 from the top of the Bezymianny. In the P–T, T–H_2O_{melt} and logfO_2–T diagrams, the dotted lines connect physicochemical values calculated from homogeneous domains within the same crystals (normal or reverse zonings; Figures 2, 3 and 5). See [1] for additional explanations on the P–T, T–H_2O_{melt} and logfO_2–T diagrams.

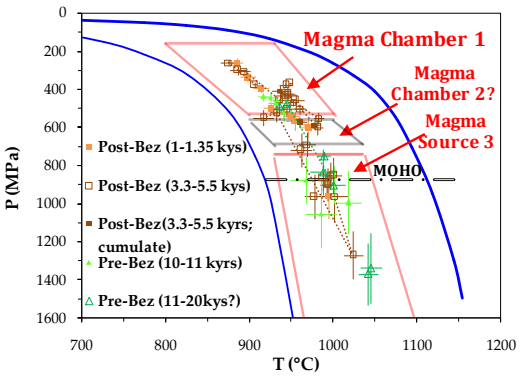

Figure 7. *Cont.*

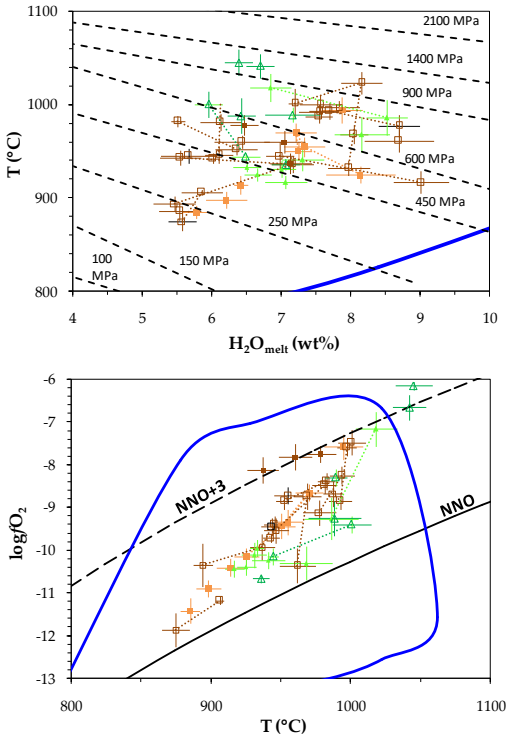

Figure 7. Amp-TB2 results for the historical and pre-historical amphiboles of the Bezymianny volcano. Magma Chambers 1 and 2, and Source 3, are reported for comparison together with the MOHO (see Figure 6 caption). The dotted lines in the P–T, T–H_2O_{melt} and logfO_2–T diagrams connect physicochemical values calculated from homogeneous zones within the same crystals (normal or reverse zonings; Figures 2, 3 and 5). All ages are related to the present time (BP). See [1] for additional explanations on the P–T, T–H_2O_{melt} and logfO_2–T diagrams.

4. The Application of Amp-TB2.1 to the Bezymianny Amphiboles and Comparison with Seismic Tomography Results

The Bezymianny volcano belongs to the Klyuchevskoy Group of volcanoes (Kamchatka, Russia), and it is the only volcano of the group which is characterized by the strong predominance of silicic eruptive products, a possible indication of the existence of large magmatic reservoir(s) underneath the volcanic edifice, where a parental basaltic magma differentiates to andesites and dacites [21,22,25,35–37]. The Bezymianny volcano began growing approximately 10,000–11,000 years BP, with periods of dormancy from 6900 to 4700 yr BP, 2750 to 2100 yr BP, 1550 to 1200 yr BP and 1000 yr BP to 1955 yr AD. The pre-historic eruptive activity at the Bezymianny formed extensive andesitic pyroclastic flow deposits and lava flows, as well as andesitic to dacitic extrusive domes [38]. The latest eruptive cycle showed a reverse silicic to more mafic trend in the chemical composition of volcanic products, from dacite in 1956 to basaltic andesite in 2012 [22,37]. It has been argued that such an acid-to-basic sequence observed in volcanic products is related to the existence of several inter-connected magma chambers at different depths [22,39]. These petrological observations were found to be consistent with independent geophysical data, e.g., [23,24,40,41]. Despite a large number of studies, the depth of the magma chamber(s) underneath the Bezymianny volcano is still an open question [20–22,25,36,37,39,42–45]. For example, [45] demonstrated, using compositional variations observed in Amp, that the key mineral of the Bezymianny volcanics, in a full range of pressures from 200 to 900 MPa, can be recovered using an older barometric formulation, i.e., [3]. However, these authors applied Amp thermobarometry only to some spot core and rim analyses, which did not allow them to identify the complete intra-crystal compositional variations related with the evolution of the magma during Amp crystallization. Below, we demonstrate that much

more details can be obtained on the evolution of the P–T conditions if a detailed Amp compositional profiling and the filtering approach described above are performed.

Figures 6 and 7 summarize the results of the application of this protocol to amphiboles from the recent, historical and pre-historical products of the Bezymianny volcano. These results are also reported in an Excel file in Supplementary Materials. Amp compositions are from [22], who published the EPMA data (mostly core–rim profiles) of 38 phenocrysts from the pre-climatic, climatic and post-climatic deposits of the activity in 1955–2010. In addition, we performed new EPMA detailed profiles on 12 selected Amp phenocrysts from the Bezymianny products erupted in 1956 and 1990, and 35 Amp crystals from andesites with historical (1–1.35 kys and 3.3–5.5 kys BP) and pre-historical ages (older than 10 kys; from lava domes extruded before the formation of the Bezymianny strato-cone, i.e., 7.8 kys BP; ages are from [38]). These samples have been previously described in [45]. Amp compositions were measured using a Cameca SX100 microprobe (University of Hannover), operated at an accelerating voltage of 15 kV and a 15 nA beam current with a beam spot of 2 μm for major elements (Supplementary Materials). Na and K were analyzed first with counting times of 8 s. The counting time for other elements was 10 s on a peak and 5 s on the background. Chlorine and fluorine were analyzed using a second-condition mode with a similar beam spot, but with a 40 nA beam current. Standards used for calibrations were the oxides Fe_2O_3, Mn_3O_4, MgO, TiO_2 and Cr_2O_3 and the minerals jadeite (Na), orthoclase (K) and wollastonite (Si and Ca). NaCl and SrF_2 were used to calibrate the halogens. In the course of each microprobe session, the analytical accuracy was verified by measuring the Smithsonian Institution's Kakanui 143, 965 reference hornblende, e.g., [26].

In the following sections, a summary of the main results and insights for the recent and old Amp-bearing products of the Bezymianny volcano are reported.

4.1. On the Characteristics of the Recent Magma-Feeding System

Figure 6 reports the Amp-TB2.1 results for the recently erupted amphiboles, together with a tomography snapshot obtained from the Vp/Vs seismic analysis of earthquakes in a particularly active period of the Bezymianny (i.e., 2005). Underneath the Bezymianny, seismicity indicates the occurrence of a first magma zone (Magma Chamber 1) at depths of 6–17 km (~160–530 MPa) and a second crustal high-Vp/Vs ratio zone (Magma Chamber 2) at depths of 18–23 km (~560–690 MPa) that, due to its proximity with the first one, can also be interpreted as an extension of Magma Chamber 1. A lower-crust–mantle source is shown underneath the nearby Klyuchevskoy volcano, and most probably feeds both volcanoes, e.g., [23,24,33,34]. The occurrence of extended magmatic zones (through Magma Chamber 1 and 2) is confirmed by our Amp-TB2.1 analysis (147–741 MPa), also showing Amp crystallization at "steady-state" conditions of 839–978 °C, 4.7–7.9 wt% H_2O_{melt} and fO_2 values from the NNO to 3 log units above. The lack of Amp-TB2.1 results at pressures of 290–360 MPa suggests the presence of two crustal chambers (Chamber A and B) connected by a narrower conduit. Figure 6 also shows normal and reverse zonings, represented by dotted lines connecting physicochemical conditions calculated for homogeneous domains within the same Amp crystal. Reverse zonings are only found within the two chambers (i.e., at 147–286 and 358–741 MPa), while normal zonings can cross all the calculated P ranges (Figures 2 and 3). In addition, the amphiboles in the ash products before the climatic event of 1956 (pre-climatic) were directly ejected from the shallower Chamber A, as they only indicate equilibrium crystallization at 184–264 MPa and lowfO_2 values of NNO ± 0.2. The following products of the 1956 climatic event show a maximum Amp crystallization P of 589 MPa, well within Magma Chamber 2, while the post-climatic amphibole extend their equilibrium crystallization pressure (and depth) down to the top of Magma Source 3. It is worth noting that more recent products of the Bezymianny (i.e., December 2017) indicate maximum Amp-TB2 depths well within this magma source at a P of 850 MPa [25], comparable in depth to the MOHO transition. Oxygen fugacity and H_2O_{melt} show generally decreasing patterns from NNO + 3 to NNO and 8.4 to 4.7 wt%, respectively, in agreement with experimental results of [21]. However, a few zonings for the deeper amphiboles in

the post-climatic products show that H_2O_{melt} can decrease with both P and T, suggesting perturbation of the system from fluids or melts coming from deeper zones (Figure 6).

4.2. On the Variation of the Magma-Feeding System through the Ages

Figure 7 reports the results of the application of the Amp-TB2.1 protocol for the historical and pre-historical products of the Bezymianny. In the P–T diagram, the locations of Magma Chamber 1 and 2 and Magma Source 3 are also reported for comparison, together with the MOHO transition. The first striking observation is that the depth of Amp crystallization is generally higher for these old products, with a minimum calculated P (262 MPa) well within Magma Chamber 1, at the bottom of the shallower Chamber A identified by the recent amphiboles (cf. Figures 6 and 7). This is observed only for the post-Bezymianny products (1–1.35 kys and 3.3–5.5 kys BP), while the minimum P of the amphiboles erupted before the genesis of the volcano (441 MPa) is located at the bottom of Magma Chamber 1 and within Chamber B, identified for the recent products (cf. Figures 6 and 7). Among the post-Bezymianny amphiboles, the younger ones (1–1.35 kys BP) mostly crystallized in the crust (261–603 MPa) and only one crystal indicates the feeding of the system from a source located at the MOHO transition. The older ones (3.3–5.5 kys BP) show a continuous increase in the crystallization depth down to the mantle (at 1273 MPa-1024 °C), although large densities of data are observed in the range of 262–601 MPa (875–982 °C) and at MOHO levels (853–963 MPa). The occurrence of the first magma-storage region at crustal levels is supported by the P–T conditions calculated on cumulus–cognate Amp crystals (homogeneous and associated with other mafic mineral inclusions; e.g., [2]) found within these 3.3–5.5 kys old products (409–584 MPa; Figure 7). Amphiboles in the products preceding the genesis of the Bezymianny (>10 kys BP) show higher values of minimum and maximum crystallization pressure (441 and 1372 MPa, respectively). These amphiboles clearly show that the feeding system was characterized by a small crustal chamber at the base of Magma Chamber 1 (441–522 MPa), fed by magma coming from a zone at crust–mantle transition (751–1056 MPa), in turn fed by deeper magmas (Figure 7).

Consistently with the recent Bezymianny amphiboles, reverse zonings are only found within the identified magma chambers, while normal zonings can connect homogeneous domains crystallized at different magmatic zones. The T–H_2O_{melt} diagram shows a much more dispersed distribution than that of the recent amphiboles (cf. Figures 6 and 7), and the zonings indicate that the amount of volatile in the melt increases with P–T only at shallow crustal depths (<400 MPa). At deeper levels, this trend is not observed, and H_2O_{melt} can follow any directions between ideal isobaric and isothermal patterns (Figure 7). Relative oxygen fugacity (ΔNNO = 0.2–3.2 log units) shows a general increase with T, like for the recent amphiboles. It is, however, worth noting that the values calculated at high-depth conditions can lead to misleading results and interpretation, as the Amp-TB2.1 fO_2 equation was calibrated with experimental amphiboles synthesized at a maximum P of 700 MPa [21]. At lower pressure, the cumulus–cognate Amps are characterized by high-fugacity values (NNO + 3; Figure 7), suggesting that, during stagnant periods, the magma system releases to the surface most of its CO_2 cargo. Indeed, in the C-H-O fluid system, fO_2 increases with the activity of H_2O, which is inversely related to the amount of CO_2, e.g., [27,45].

5. Final Remarks

This article shows that the application of the proposed protocol is essential to quantify the "steady-state" conditions of amphibole crystallization (through the identification of homogeneous crystals or intra-crystal domains) and to retrieve reliable estimations on the depths and sizes of the magma-storagelevels. Heterogeneous domains can be eventually considered for a qualitative analysis to estimate at which extent the physicochemical parameters can "apparently" change during kinetic (disequilibrium) processes, such as magma ascent, mixing and convection.However, the users should be aware that the Amp-TB2 model has been calibrated at equilibrium conditions where the physicochemical and compositional parameters are assumed to be constant for a long time (ideally infinite), and

that it can provideunpredictable results when the sub-volcanic processes are too fast for allowing the amphibole-melt chemical equilibrium to be sufficiently approached. This phenomenon mostly affects the estimated P (and depth) values.For instance, Kiss et al. [46] reported Amp phenocryst domains showing oscillatory zonings with large decreases and increases in major elements over intra-crystal distances of a few microns, associated with large P variations (~100–300 MPa).In addition, the applicationof Amp thermobarometry to four cooling experiments performed at 150 MPa by Shea and Hammer [47] shows slight temperature overestimations (6–27 °C; approximately consistent with theuncertainty of Amp-TB2) and pronounced pressure overestimations of ~100–200% [6].

Overall, the Amp-TB2.1 analysis of the recent, historical and pre-historical products of the Bezymianny indicates a very dynamic feeding system changing frequently through time. The magma is stored at shallow crust levels during recent activity periods, and the depth of the magma withdrawn by the volcano generally increases with age. The recent amphiboles of the Bezymianny indicates that the first explosive events after a period of quiescence are triggered by magmatic processes occurring at the shallower storage levels in the crust, similarly to other volcanoes, e.g., [2,3]. We suggest that, in order to mitigate the volcanic risk, particular care should be taken in monitoring the seismicity of active volcanoes at these levels during quiescent periods (previously constrained through thermobarometry, petrology, geochemistry and geophysics). In particular, a rigorous application of the Amp-TB2 protocol can bring clarity to the depth of these shallow-crust storage regions, facilitating the interpretation of seismic volcano–tectonic events occurring underneath volcanoes, e.g., [2,3].

Supplementary Materials: The following are available online at https://www.mdpi.com/article/10.3390/min13111394/s1, Table S1. Amp-TB2.1.xlsx and Bez. Amp-TB2.1 results.xlsx.

Author Contributions: Conceptualization, F.R. and F.H.; methodology, R.R.A.; software, F.R.; validation, F.R., R.R.A., A.Y.O. and F.H.; formal analysis, F.R.; investigation, F.R. and R.R.A.; resources, R.R.A. and A.Y.O.; data curation, F.R. and R.R.A.; writing—original draft preparation, F.R.; writing—review and editing, F.R.; visualization, R.R.A.; supervision, F.H. and A.Y.O.; project administration, F.R.; funding acquisition, F.R. All authors have read and agreed to the published version of the manuscript.

Funding: This research was funded by the Alexander von Humboldt-Stiftung, with a research fellowship to the author, and the Deutsche Forschungsgemeinschaft (DFG), grant codes RI 3065/2-1 and RI 3065/2-2.

Data Availability Statement: Data supporting reported results can be found in the Supplementary Materials, Amp-TB2.xlsx.

Acknowledgments: The scientific staff at the Institut für Mineralogie at LUH is thanked for their continuous support.

Conflicts of Interest: The authors declare no conflict of interest.

References

1. Ridolfi, F. Amp-TB2: An Updated Model for Calcic Amphibole Thermo-barometry. *Minerals* **2021**, *11*, 32A. [CrossRef]
2. Ridolfi, F.; Puerini, M.; Renzulli, A.; Menna, M.; Toulkeridis, T. The magmatic feeding system of El Reventador volcano (Sub-Andean zone, Ecuador) constrained by texture, mineralogy and thermobarometry of the 2002 erupted products. *J. Volcanol. Geotherm. Res.* **2008**, *176*, 94–106. [CrossRef]
3. Ridolfi, F.; Renzulli, A.; Puerini, M. Stability and chemical equilibrium of amphibole in calc-alkaline magmas: An overview, new thermobarometric formulations and application to subduction-related volcanoes. *Contrib. Mineral. Petrol.* **2010**, *160*, 45–66. [CrossRef]
4. Ridolfi, F.; Renzulli, A. Calcic amphiboles in calc-alkaline and alkaline magmas: Thermobarometric and chemometric empirical equations valid up to 1130 °C and 2.2 GPa. *Contrib. Mineral. Petrol.* **2012**, *163*, 877–895. [CrossRef]
5. Ridolfi, F.; Renzulli, A.; Perugini, D.; Cesare, B.; Braga, R.; Del Moro, S. Unravelling the complex interaction between mantle and crustal magmas encoded in the lavas of San Vincenzo (Tuscany, Italy). Part I: Petrography and Thermobarometry. *Lithos* **2016**, *244*, 218–232. [CrossRef]

6. Gorini, A.; Ridolfi, F.; Piscaglia, F.; Taussi, M.; Renzulli, A. Application and reliability of calcic amphibole thermobarometry as inferred from calc-alkaline products of active geothermal areas in the Andes. *J. Volcanol. Geotherm. Res.* **2018**, *358*, 58–76. [CrossRef]
7. Ridolfi, F.; Zanetti, A.; Renzulli, A.; Perugini, D.; Holtz, F.; Oberti, R. AMFORM, a new mass-based model for the calculation of the unit formula of amphiboles from Electron Micro-Probe analyses. *Am. Mineral.* **2018**, *103*, 1112–1125. [CrossRef]
8. Benz, H.M.; Chouet, B.A.; Dawson, P.B.; Lahr, J.C.; Page, R.A.; Hole, J.A. Three-dimensional P and S wave velocity structure ofRedoubt Volcano, Alaska. *J. Geophys. Res.* **1996**, *101*, 8111–8128. [CrossRef]
9. Aspinal, W.P.; Miller, A.D.; Lynch, L.L.; Latchman, J.L.; Stewart, R.C.; White, R.A.; Power, J.A. Soufriére Hills eruption, Montserrat, 1995–1997: Volcanic earthquake locations and fault planesolutions. *Geophys. Res. Lett.* **1998**, *25*, 3397–3400. [CrossRef]
10. Lees, J.M. Seismic tomography of magmatic systems. *J. Volcanol. Geotherm. Res.* **2007**, *167*, 37–56. [CrossRef]
11. Moran, S.C.; Malone, S.D.; Qamar, A.I.; Thelen, W.; Wright, A.K.; Caplan-Auerbach, J. Seismicity associated with renewed domebuildingat Mount St. Helens, 2004–2005. In *A Volcano Rekindled: The Renewederuption of Mount St. Helens, 2004–2006*, 1st ed.; Sherrod, D.R., Scott, W.E., Stauffer, P.H., Eds.; U.S. Geological Survey Professional Paper; U.S. Geological Survey: Reston, VA, USA, 2008; Volume 1, Chapter 2; pp. 27–60.
12. Innocenti, S.; del Marmol, M.-A.; Voight, B.; Andreastuti, S.; Furman, T. Textural and mineral chemistry constraints on evolution of Merapi Volcano, Indonesia. *J. Volcanol. Geotherm. Res.* **2013**, *261*, 20–37. [CrossRef]
13. Trua, T.; Marani, M.; Barca, D. Lower crustal differentiation processes beneath a back-arc spreading ridge (Marsili seamount, Southern Tyrrhenian Sea). *Lithos* **2014**, *190–191*, 349–362. [CrossRef]
14. Burns, D.H.; de Silva, S.L.; Tepley, F., III; Schmitt, A.K.; Loewen, M.W. Recording the transition from flare-up to steady-state arc magmatism at the Purico–Chascon volcanic complex, northern Chile. *Earth Plan. Sci. Lett.* **2015**, *422*, 75–86. [CrossRef]
15. Harangi, S.; Novák, A.; Kiss, B.; Seghedi, I.; Lukács, R.; Szarka, L.; Wesztergom, V.; Metwaly, M.; Gribovszki, K. Combined magnetotelluric and petrologic constrains for the nature of the magma storage system beneath the Late Pleistocene Ciomadul volcano (SE Carpathians). *J. Volcanol. Geotherm. Res.* **2015**, *290*, 82–96. [CrossRef]
16. Dobretsov, N.L.; Simonov, V.A.; Koulakov, I.Y.; Kotlyarov, A.V. Migration of fluids and melts in subduction zones and general aspects of thermophysical modeling in geology. *Rus. Geol. Geophys.* **2017**, *58*, 571–585. [CrossRef]
17. Mata, J.; Martins, S.; Mattielli, N.; Madeira, J.; Faria, B.; Ramalho, R.S.; Silva, P.; Moreira, M.; Caldeira, R.; Moreira, M. The 2014-15 eruption and the short-term geochemical evolution of the Fogo volcano (Cape Verde): Evidence for small-scale mantle heterogeneity. *Lithos* **2017**, *288–289*, 91–107. [CrossRef]
18. Nagasaki, S.; Ishibashi, H.; Suwa, Y.; Yasuda, A.; Hokanishi, N.; Ohkura, T.; Takemura, K. Magma reservoir conditions beneath Tsurumi volcano, SW Japan: Evidence from amphibole thermobarometry and seismicity. *Lithos* **2017**, *278–281*, 153–165. [CrossRef]
19. Stechern, A.; Just, T.; Holtz, F.; Blume-Oeste, M.; Namur, O. Decoding magma plumbing and geochemical evolution beneath the Lastarria volcanic complex (Northern Chile)—Evidence for multiple magma storage regions. *J. Volcanol. Geotherm. Res.* **2017**, *338*, 25–45. [CrossRef]
20. Almeev, R.R.; Ariskin, A.A.; Ozerov, A.Y.; Kononkova, N.N. Problems of the stoichiometry and thermobarometry of magmatic amphiboles: An example of hornblende from the andesites of Bezymianny volcano, Eastern Kamchatka. *Geochem. Int.* **2002**, *40*, 723–738.
21. Almeev, R.R.; Holtz, F.; Ariskin, A.A.; Limura, J.-I. Storage conditions of Bezymianny Volcano parental magmas: Results of phase equilibria experiments at 100 and 700 MPa. *Contrib. Mineral. Petrol.* **2013**, *166*, 1389–1414. [CrossRef]
22. Turner, S.J.; Izbekov, P.; Langmuir, C. The magma plumbing system of Bezymianny Volcano: Insights from a 54 year time series of trace element whole-rock geochemistry and amphibole compositions. *J. Volcanol. Geotherm. Res.* **2013**, *263*, 108–121. [CrossRef]
23. Koulakov, I.; Gordeev, E.I.; Dobretsov, N.L.; Vernikovsky, V.A.; Senyukov, S.; Jakovlev, A.; Jaxybulatov, K. Rapid changes in magma storage beneath the Klyuchevskoy group of volcanoes inferred from time-dependent seismic tomography. *J. Volcanol. Geotherm. Res.* **2013**, *263*, 75–91. [CrossRef]
24. Koulakov, I.; Abkadyrov, I.; Al Arifi, N.; Deev, E.; Droznina, S.; Gordeev, E.I.; Jakovlev, A.; El Khrepy, S.; Kulakov, R.I.; Kugaenko, Y.; et al. Three different types of plumbing system beneath the neighboring active volcanoes of Tolbachik, Bezymianny, and Klyuchevskoy in Kamchatka. *J. Geophys. Res. Solid Earth* **2017**, *122*, 3852–3874. [CrossRef]
25. Davydova, V.O.; Shcherbakov, V.D.; Plechov, P.Y.; Koulakov, I.Y. Petrological evidence of rapid evolution of the magma plumbing systemofBezymianny volcano in Kamchatka before the December 20th, 2017 eruption. *J. Volcanol. Geotherm. Res.* **2022**, *421*, 107422. [CrossRef]
26. Liu, Y.; Yang, W.; Zhang, C.; Bao, Z.; Wu, S.; Almeev, R.A.; Ridolfi, F.; Oberti, R. New Compositional and Structural Constraints on the Smithsonian Microanalytical Reference Materials: Amphiboles from Kakanui and Arenal. *Geostand. Geoanal. Res.* **2023**, *47*, 595–608. [CrossRef]
27. Scaillet, B.; Evans, B.W. The 15 June 1991 eruption of Mount Pinatubo; I, Phase equilibria and pre-eruption P-T-fO_2-fH_2conditions of the dacite magmas. *J. Petrol.* **1999**, *40*, 381–411. [CrossRef]
28. Chakraborty, S. Rates and mechanisms of Fe-Mg interdiffusion in olivine at 980°–1300° C. *J. Geophys. Res. Solid Earth* **1997**, *103*, 12317–12331. [CrossRef]
29. Costa, F.; Chakraborty, S.; Dohmen, R. Diffusion coupling between trace and major elements and a model for calculation of magma residence times using plagioclase. *Geochem. Cosmochem. Acta* **2003**, *67*, 2189–2200. [CrossRef]

30. Costa, F.; Dohmen, R.; Chakraborty, S. Time scales of magmatic processes from modeling the zoning patterns of crystals. *Rev. Mineral. Geochem.* **2008**, *69*, 545–594. [CrossRef]
31. Costa, F.; Shea, T.; Ubide, T. Diffusion chronometry and the timescales of magmatic processes. *Nature Rev. Earth Environ.* **2020**, *1*, 201–214. [CrossRef]
32. Zhang, C.; Koepke, J.; Wang, L.-X.; Wolff, P.E.; Wilke, S.; Stechern, A.; Almeev, R.A.; Holtz, F. A Practical Method for Accurate Measurement of Trace Level Fluorine in Mg- and Fe-Bearing Minerals and Glasses Using Electron Probe Microanalysis. *Geostand. Geoanal. Res.* **2016**, *40*, 351–363. [CrossRef]
33. Thelen, W.; West, M.; Senyukov, S. Seismic characterization of the fall 2007 eruptive sequence at Bezymianny Volcano, Russia. *J. Volcanol. Geotherm. Res.* **2010**, *194*, 201–213. [CrossRef]
34. William, B.F.; Shapiro, N.M.; Gusev, A.A. Progressive reactivation of the volcanic plumbing system beneath Tolbachik volcano (Kamchatka, Russia) revealed by long-period seismicity. *Earth Plan. Sci. Lett.* **2018**, *493*, 47–56.
35. Bogoyavlenskaya, G.E.; Braitseva, O.A.; Melekestsev, I.V.; Maksimov, A.P.; Kiriyanov, V.X.; Dan Miller, C. Catastrophic eruptions of the directed-blast type at Mount St. Helens, Bezymianny and Shiveluch volcanoes. *J. Geodyn.* **1985**, *3*, 189–218. [CrossRef]
36. Ozerov, A.A.; Ariskin, A.A.; Kyle, P.; Bogoyavlenskaya, G.E.; Karpenko, S.F. Petrological-geochemical model for genetic relationships between basaltic and andesitic magmatism of Klyuchevskoy and Bezymianny volcanoes, Kamchatka. *Petrology* **1997**, *5*, 550–569.
37. Davydova, V.O.; Shcherbakov, V.D.; Plechov, P.X.; Perepelov, A.B. Petrology of mafic enclaves in the 2006–2012 eruptive products of Bezymianny Volcano, Kamchatka. *Petrology* **2017**, *25*, 592–614. [CrossRef]
38. Braitseva, O.A.; Melekestsev, I.V.; Bogoyavlenskaya, G.E.; Maksimov, A.P. Bezymianny: Eruptive history and dynamics. *Volcanol. Seismol.* **1991**, *12*, 165–195.
39. Shcherbakov, V.; Plechov, P.; Izbekov, P.; Shipman, J. Plagioclase zoning as an indicator of magma processes at Bezymianny Volcano, Kamchatka. *Contrib. Mineral. Petrol.* **2011**, *162*, 3–99. [CrossRef]
40. Koloskov, A.V.; Ananyev, V.V. New Data on the Age, Material Composition, and Geological Structure of the Central Kamchatka Depression (CKD). Part 2. The Mineralogical Composition of Volcanic Rocks and Mantle Xenoliths. Toward a Petrologic Model. *J. Volcanol. Seism.* **2020**, *14*, 145–165. [CrossRef]
41. Koulakov, I.; Plechov, P.; Mania, R.; Walter, T.R.; Smirnov, S.Z.; Abkadyrov, I.; Jakovlev, A.; Davydova, V.; Senyukov, S.; Bushenkova, N.; et al. Anatomy of the Bezymianny volcano merely before an explosive eruption on 20.12.2017. *Sci. Rep.* **2021**, *11*, 1758. [CrossRef]
42. Maksimov, A.P.; Kadik, A.A.; Korovushkina, E.Y.; Ivanov, B.V. Crystallization of an andesite melt with a fixed water content at pressures up to 12 kbar. *Geochem. Int.* **1978**, *15*, 20–29.
43. Plechov, P.; Tsai, A.; Shcherbakov, V.; Dirksen, O. Opacitization conditions of hornblende in Bezymyannyi volcano andesites (March 30, 1956 eruption). *Petrology* **2008**, *16*, 19–35. [CrossRef]
44. Shcherbakov, V.D.; Neill, O.K.; Izbekov, P.E.; Plechov, P.Y. Phase equilibria constraints on pre-eruptive magma storage conditions for the 1956 eruption of Bezymianny Volcano, Kamchatka, Russia. *J. Volcanol. Geotherm. Res.* **2013**, *263*, 132–140. [CrossRef]
45. Almeev, R.R.; Kimura, J.-I.; Ariskin, A.A.; Ozerov, A.Y. Decoding crystal fractionation in water-rich calc-alkaline magma from Bezymianny volcano, Kamchatka, Russia, using mineral and bulk rock chemistry. *J. Volcanol. Geotherm. Res.* **2013**, *263*, 141–171. [CrossRef]
46. Kiss, B.; Harangi, S.; Ntaflos, T.; Mason, P.R.D.; Pál-Molnár, E. Amphibole perspective to unravel pre-eruptive processes and conditions in volcanic plumbing systems beneath intermediate arc volcanoes: A case study from Ciomadul volcano (SECarpathians). *Contrib. Mineral. Petrol.* **2014**, *167*, 986. [CrossRef]
47. Shea, T.; Hammer, J.E. Kinetics of cooling and decompression-induced crystallizationin hydrous mafic-intermediate magmas. *J. Volcanol. Geotherm. Res.* **2013**, *260*, 127–145. [CrossRef]